

Two-Dimensional Patterns in Bacterial Veils Arise from Self-generated, Three-Dimensional Fluid Flows

N.G. Cogan^a, C.W. Wolgemuth^{b,*}

^aDepartment of Mathematics, Florida State University, 208 Love Building, Tallahassee, FL 32317, USA

^bDepartment of Cell Biology and Center for Cell Analysis and Modeling, University of Connecticut Health Center, 263 Farmington Avenue, Farmington, CT 06030, USA

Received: 5 October 2009 / Accepted: 11 March 2010
© Society for Mathematical Biology 2010

Abstract The behavior of collections of oceanic bacteria is controlled by metabolic (chemotaxis) and physical (fluid motion) processes. Some sulfur-oxidizing bacteria, such as *Thiovulum majus*, unite these two processes via a material interface produced by the bacteria and upon which the bacteria are transiently attached. This interface, termed a bacterial veil, is formed by exo-polymeric substances (EPS) produced by the bacteria. By adhering to the veil while continuing to rotate their flagella, the bacteria are able to exert force on the fluid surroundings. This behavior induces a fluid flow that, in turn, causes the bacteria to aggregate leading to the formation of a physical pattern in the veil. These striking patterns are very similar in flavor to the classic convection instability observed when a shallow fluid is heated from below. However, the physics are very different since the flow around the veil is mediated by the bacteria and affects the bacterial densities.

In this study, we extend a model of a one-dimensional veil in a two-dimensional fluid to the more realistic two-dimensional veil in a three-dimensional fluid. The linear stability analysis indicates that the Peclet number serves as a bifurcation parameter, which is consistent with experimental observations. We also solve the nonlinear problem numerically and are able to obtain patterns that are similar to those observed in the experiments.

Keywords Fluid/structure · Biofilm · Pattern formation · Bacterial veils · Instability · Boundary integral method

1. Introduction

Understanding the underlying processes which influence our global climate requires understanding the global carbon cycle, as atmospheric carbon dioxide is the major player in global warming. The metabolism of microorganisms found in the oceans is a significant

*Corresponding author.

E-mail address: cwolgemuth@uchc.edu (C.W. Wolgemuth).

contributor to the carbon cycling. Especially, many coastal sediments in shallow water show a microbial activity which sometimes even surpasses the metabolic activity of rain forests (e.g., if measuring respiration rates per unit area). As marine water contains large amounts of sulfate, a major part of sediment microorganisms are specialized in metabolizing sulfur compounds like sulfide, elemental sulfur, or sulfate (Berglen et al., 2004). These bacteria link the global carbon cycle with the global sulfur cycle. Thus, it is of interest to understand the processes of the sulfur cycle and their influence on the carbon cycle.

Biological observations of certain sulfur-oxidizing bacteria have indicated complex interactions between the bacteria, the surrounding fluid and the metabolic processes. In shallow water, these bacteria tend to aggregate by aerotaxis at an optimal oxygen concentration (around $2 \mu\text{M}$ oxygen for *Thioturbo danicus*). This typically occurs anywhere from zero to ten millimeters above the sediment floor (Thar and Kühl, 2006). Once aggregated, the bacteria can attach to sediment and other bacteria via a mucous stalk. The mucous stalks from neighboring bacteria can become stuck together, which produces a cohesive whitish veil. The veil acts to anchor the bacteria at a relatively constant depth (Fenchel and Glud, 1998; Thar and Kühl, 2002, 2003; Thar and Fenchel, 2001). While anchored to the veil, the bacteria exert force on the surrounding fluid by rotating their flagella, which has the effect of rotating their bodies and pulling fluid past them. However, the bacteria are only transiently attached to the veil; bacteria frequently detach from the veil, typically on the upper, oxic side, and swim in a U-shaped pattern that eventually brings them back to the veil. The fluid flow created by the anchored bacteria exerts force on the free-swimming bacteria and the veil. The veil undergoes a transition from a uniform distribution into either stripes or spotted patterns that are similar to convection rolls and cells in appearance, although the physical mechanism is quite different (Muyzer et al., 2005; Thar and Kühl, 2002, 2003; Thar and Fenchel, 2001; Fenchel and Glud, 1998).

In this paper, we extend the analysis of a one-dimensional veil in a two-dimensional fluid to a two-dimensional veil in a three-dimensional fluid. This model considers an idealized system that mimics the experiments done under laboratory conditions using a benthic gradient chamber (Thar and Kühl, 2002) (Fig. 1) and presumes that the patterns that are observed in this system are dominated by the interaction between the fluid flow and the bacteria (i.e., our model does not take into account chemotactic effects that might arise from depleted oxygen zones surrounding small aggregates of bacteria). We find that the model captures the pattern formation that is observed experimentally, which shows that the physical interaction between the bacteria and the fluid are sufficient to drive patterns in this system.

In the first section, we review the biological processes that underlie the formation and dynamics of the polymer veil. We also describe two previous models that have been introduced to study the pattern formation in this system. Sections 3–5 describe the development of a three-dimensional model of the dynamics of the fluid motion and bacterial aggregation. This model depends on four physical and experimentally measurable parameters: the height of the veil, the swimming speed of the bacteria, a bacterial diffusion coefficient, and the ratio of the rate that the bacteria attach to the veil to the detachment rate. The resulting model is analyzed by first examining the linearized problem. The nonlinear problem is then analyzed computationally. The results indicate that our model captures the relevant biological observations. Finally, we discuss the results and indicate directions for future investigations.

Thar and Kühl, 2002). Depending on the bacterial species, the voids can form either rolls or regularly-spaced patterns.

Thar and Kühl developed a controllable laboratory setup that mimics the veil formation that is seen in the ocean (Thar and Kühl, 2002). Briefly, samples of bacterial veils were inoculated into a chamber where a layer of sand was supported by a nylon mesh over liquid sulfitic medium. After 2 to 3 days, several small veils (20 mm \times 20 mm in size) formed on the sand surface. Successive veils then formed above the existing veil. After roughly one week, a single, continuous veil was formed that spanned the chamber at a constant height above the sand. This veil did not show any inhomogeneities, but within 2 days a regular pattern of evenly spaced holes formed that were roughly 0.3 mm in diameter. Microscopic observation showed that the bacteria were attached to the top of the veil and spaced at roughly 10–20 μ m apart. A schematic of this process is shown in Fig. 1.

The material interface on which the bacteria are attached is composed of a polymeric gel formed from the bacterial products. In turn, the presence of the veil affects the fluid velocity (and hence the bacterial distribution) since the veil acts as a semipermeable layer that interacts with the fluid through the interphase (fluid/polymer) drag.

A model for the coupled fluid and bacterial motion was derived previously (Cogan and Wolgemuth, 2005). This model was posed in two dimensions, where the veil is a one-dimensional interface aligned with the x -axis and immersed in the two-dimensional fluid. The model does not account for the production of the veil, but assumes that the veil is located at a fixed height, h , above the ocean floor. The bacteria are considered to be either adhered to the veil (bound) or swimming above the veil (free). To simplify the analysis, it is assumed that there is no interaction between the fluid and the veil. Rather, the fluid motion is created by forces from the bound bacteria, and this fluid motion affects the swim path of the free bacteria. Free bacteria bind to the veil at a rate τ_f . As bacteria swimming near the veil are observed to swim in parabolic trajectories that bring the bacteria back to the veil (Thar and Kühl, 2003), it is presumed that this rate represents the average time between release from the veil and return to the veil. It is also likely that this rate depends on the details of the fluid flow; however, we treat this rate as a constant. Bound bacteria break free of the veil at a rate τ_b .

The free bacteria swim and are advected by the fluid. Free swimming is modeled as a diffusive term, with diffusion coefficient, D_f . Instead of treating chemotaxis explicitly, we assume that the chemotaxis of the bacteria tends to move the bacteria back to the veil. Therefore, free cells swim an average height, δ , above the veil. This treatment effectively averages over the vertical motion of the bacteria, and we only consider advection parallel to the veil, simplifying the equations substantially. Denoting the density of free and bound bacteria as n_f and n_b , respectively, we find that the densities are determined by

$$\frac{\partial n_b}{\partial t} = -\frac{1}{\tau_b}n_b + \frac{1}{\tau_f}n_f, \quad (1)$$

$$\frac{\partial n_f}{\partial t} = D_f \Delta n_f - \frac{\partial n_f \mathbf{v}_{x,\delta}}{\partial x} + \frac{1}{\tau_b}n_b - \frac{1}{\tau_f}n_f. \quad (2)$$

Here, $\mathbf{v}_{x,\delta}$ denotes the x -component of the fluid velocity evaluated at the height δ above the veil. In these equations, the time rate of change of the concentration of bound bacteria is balanced by detachment and attachment, whereas the time rate of change of the free

bacteria is balanced by swimming (e.g., diffusion), advection by the fluid parallel to the veil, and detachment/attachment.

Scaling the fluid motion using a typical veil height and the bacterial velocity scales leads to a Reynolds' number on the order of 10^{-1} . This scaling indicates that the fluid dynamics are dominated by viscous forces. Rather than deal with the nonlinear Navier–Stokes equations, we approximate the fluid dynamics with the incompressible Stokes equation:

$$\mu \Delta \mathbf{v} - \nabla p = \mathbf{K}(\mathbf{x}), \quad (3)$$

$$\nabla \cdot \mathbf{v} = 0. \quad (4)$$

The force, \mathbf{K} on the right-hand side represents the force that the bound bacteria exerts on the fluid as they rotate. We assume that this force is down and proportional to the number of bound bacteria, $\mathbf{K} = -\alpha n_b \mathbf{y}$, where \mathbf{y} is a unit vector oriented orthogonally to the veil (e.g., orthogonal to the x -axis).

Although the inertial terms are neglected, this is a standard simplification. Stokes equations inherit a range of qualities that are not consistent with the nonlinear problem. In particular, Stokes equations are “time-reversible” and linear. Reversibility implies that periodic forcing does not impart fluid motion on average. In our case, the forces on the fluid are not periodic (or symmetric), so this does not restrict our results. More importantly, the model described above and extended below, rests on the transformation of the partial differential equation into integral equations by exploiting the linearity of the equations. Thus, our analysis is not directly applicable to studying finite Reynolds' number flows. However, it is well established that low Reynolds' number flows are well approximated by Stokes equations in a variety of settings (Batchelor, 1967).

Using the boundary integral method (Pozrikidis, 1992), we represent the fluid motion as an integral over the entire veil,

$$\mathbf{v}_i = \frac{1}{4\pi\mu} \int dx_0 \mathbf{G}_{ij}(\mathbf{x}, \mathbf{x}_0) \mathbf{K}(\mathbf{x}), \quad (5)$$

where \mathbf{G}_{ij} is the Green's function (or Stokeslet) relating the flow at \mathbf{x} generated by forces at location \mathbf{x}_0 . The boundary integral method rests on the properties of the Green's function. Fortunately, this can be calculated for a wide variety of domains (Blake, 1971; Pozrikidis, 1992; Cortez, 2001).

We note that the boundary conditions for all variables were periodic in the x -direction. No-slip boundary conditions were imposed on the fluid at $z = 0$ by our choice of Green's function. Since we have assumed that the veil does not influence the fluid, there are no boundary conditions to be imposed at the veil. The analytic form of the velocity can be recovered in this case by direct integration. We find that near a hole in the veil the fluid dynamics tends to push free bacteria back onto the veil away from the hole. This feedback causes the population to aggregate in regularly spaced regions. Presumably, the gel deteriorates between these population peaks, reinforcing the formation of holes. However, this analysis did not address the formation of two-dimensional patterns. Therefore, in the present investigation, we extend the analysis of the model to a two-dimensional veil immersed in a three-dimensional fluid. We show that aggregation can form both striped and spotted patterns. The Peclet number acts as a bifurcation parameter with veils higher above the surface tending to display honeycombed patterns.

The mechanism for pattern formation given here differs from another model (Thar and Kühl, 2006) where a phenomenological description of the interaction between bacteria at the veil was considered. This model assumed that bacteria that were close together were attracted to each other, possibly due to hydrodynamic coupling or oxygen depletion effects. At larger distances, though, the fluid flow due to the bacteria was assumed to lead to repulsion. A sombrero-shaped interaction function was used to describe the bacterial interactions, and a generic “environmental parameter,” q , was defined to define the lengthscale at which the repulsion dominated. Therefore, this parameter is intended to encompass the processes that drive bacterial aggregation (fluid dynamics and chemotaxis). The steady-state distribution of bacteria is then determined by maximizing the sum of the contribution of the environmental parameter over all the bound bacteria. Simulation results using different values of the environmental parameter and initial bacterial densities indicate that the model can capture many of the observed patterns in bacterial veils. This model, however, is purely phenomenological and does not provide a clear method for determining the value of q in terms of the known biology/physics.

The model presented here uses experimentally measurable parameters (forces on the fluid, average swimming trajectories, etc.) and an accurate description of the fluid flow to account for the pattern formation. We do not model the effects of localized oxygen depletion by the bacteria, but rather show that hydrodynamic forces on the swimming bacteria can explain the observed patterns.

3. Extended model

In this section, we describe the extension of the one-dimensional veil in a two-dimensional fluid to determine the dynamics of a two-dimensional veil in a three-dimensional fluid. The model follows from the previous model, although the analysis is complicated by the added dimensionality.

As in the one-dimensional veil problem, we consider the experimental system shown in Fig. 1. In these experiments, a continuous bacterial veil was observed to form at a uniform height (ca. a few millimeters) above the marine sediment, and after a few days this continuous veil became perforated with evenly spaced holes. We do not model the initial formation of the veil, but rather consider that at time $t = 0$ a continuous veil structure exists at a fixed height h above the marine sediment. We consider a three-dimensional fluid with a two-dimensional veil, where the veil is parallel to the x - y plane and located at $z = 0$ (see Fig. 1). Free-swimming bacteria attach to the veil with a rate $1/\tau_f$. Bound bacteria detach at a rate $1/\tau_b$. Upon detaching, the bacteria release from the veil on the upper side at a random orientation with respect to the veil. Aerotaxis brings the bacteria back to the veil; however, fluid flows can also transport the free-swimming bacteria. We assume that on average the bacteria swim a height δ above the veil. In all, therefore, the free swimming bacteria diffuse (due to the random release orientation) and are advected by the flow, which is considered to be the fluid flow at height δ above the veil. This leads to an analogous set of equations to the one-dimensional veil system, where the dynamic equations governing the bacterial populations are

$$\frac{\partial n_b}{\partial t} = -\frac{1}{\tau_b}n_b + \frac{1}{\tau_f}n_f, \quad (6)$$

$$\frac{\partial n_f}{\partial t} = D_f \Delta n_f - \left(\frac{\partial n_f \mathbf{v}_{x,\delta}}{\partial x} + \frac{\partial n_f \mathbf{v}_{y,\delta}}{\partial y} \right) + \frac{1}{\tau_b}n_b - \frac{1}{\tau_f}n_f, \quad (7)$$

where $\mathbf{v}_{x,\delta}$ and $\mathbf{v}_{y,\delta}$ are the x and y -components of the fluid velocity at a height δ above the veil. The fluid motion is governed by the three-dimensional form of Eqs. (3)–(4).

Following Cogan and Wolgemuth (2005), we rescale the equations by $\hat{x} = x/h$, $\hat{t} = D_f t/h^2$, and the equilibrium concentration of bound bacteria n_0 , which leads to a dimensionless set of equations with four control parameters, the two rate constants, a Peclet number P_c , and the dimensionless height that the bacteria swim above the veil. We denote the scaled rate constants as $k_- = \tau_D/\tau_b$ and $k_+ = \tau_D/\tau_f$, where the characteristic time scale is $\tau_d = h^2/D_f$. The dimensionless swimming height is denoted $\hat{\delta} = \delta/h$ and $P_c = \alpha h^2 n_0 / 8\pi D_f \mu$ defines the relative importance of advection to diffusion. Changing the dependent and independent variables to the dimensionless variables (and dropping the hats), we obtain

$$\frac{\partial n_b}{\partial t} = -k_- n_b + k_+ n_f, \quad (8)$$

$$\frac{\partial n_f}{\partial t} = \Delta n_f - P_c \left(\frac{\partial n_f \mathbf{v}_{x,\delta}}{\partial x} + \frac{\partial n_f \mathbf{v}_{y,\delta}}{\partial y} \right) + k_- n_b - k_+ n_f. \quad (9)$$

The dimensionless velocity can be calculated analytically using the boundary integral method (Pozrikidis, 1992),

$$\mathbf{v}(\mathbf{x}) = -\alpha \int_{-\infty}^{\infty} \int_{-\infty}^{\infty} n_b(\mathbf{x}_0) [G_{xz}(\mathbf{x}, \mathbf{x}_0) \hat{\mathbf{x}} + G_{yz}(\mathbf{x}, \mathbf{x}_0) \hat{\mathbf{y}}] dx_0 dy_0, \quad (10)$$

where G_{xz} and G_{yz} are the components of the Green's function tensor that give the velocity in x and y when a force acts on the fluid in the z direction. We have again assumed that the force on the fluid arising from the attached bacteria is proportional to the density of bound bacteria, with proportionality constant denoted α . This force is again aligned perpendicular to the veil.

For flow bounded by a plane wall, Lorentz showed that these Green's functions can be written in terms of the Stokeslet, the doublet tensor, and the dipole tensor (Lorentz, 1907). This has also been demonstrated elsewhere (Blake, 1971). For a nice review of the topic, see also Pozrikidis (1992). These Green's functions computed at the height δ above the veil are

$$G_{xz} = \frac{\delta(x-x_0)}{[(x-x_0)^2 + (y-y_0)^2 + (z-z_0)^2]^{3/2}} - \frac{\delta(x-x_0)}{[(x-x_0)^2 + (y-y_0)^2 + (z-z_l)^2]^{3/2}} - \frac{6(1+\delta)(x-x_0)(z-z_l)}{[(x-x_0)^2 + (y-y_0)^2 + (z-z_l)^2]^{5/2}}, \quad (11)$$

which can be rewritten in terms of derivatives of x and z as

$$G_{xz} = -\frac{\partial}{\partial x} \left(\frac{\delta}{[(x-x_0)^2 + (y-y_0)^2 + (z-z_0)^2]^{1/2}} \right) + \left(\delta \frac{\partial}{\partial x} - 2(1+\delta) \frac{\partial^2}{\partial x \partial z} \right) \left(\frac{1}{[(x-x_0)^2 + (y-y_0)^2 + (z-z_l)^2]^{1/2}} \right). \quad (12)$$

Here, the subscript I denotes the image charge points about the $z = 0$ axis, and we have used that $x_I = x_0$ and $y_I = y_0$. Note that the Green's function given in Eq. (11) satisfies no-slip conditions at $z = 0$; i.e., when $\delta = -1$.

Likewise, the yz component is

$$G_{yz} = -\frac{\partial}{\partial y} \left(\frac{\delta}{[(x-x_0)^2 + (y-y_0)^2 + (z-z_0)^2]^{1/2}} \right) + \left(\delta \frac{\partial}{\partial y} - 2(1+\delta) \frac{\partial^2}{\partial y \partial z} \right) \left(\frac{1}{[(x-x_0)^2 + (y-y_0)^2 + (z-z_I)^2]^{1/2}} \right). \quad (13)$$

Equations (8), (9), and (10) give a closed set of nonlinear equations for the concentrations of free and bound bacteria, and the fluid velocity. We are interested in how the parameters effect the development of patterns on the veil. Because we are not treating the polymer concentration explicitly, we assume that if there are regions without bound bacteria, the polymer degrades leaving holes.

In the next two sections, we consider the stability of a uniform distribution of bound bacteria to perturbations. We first linearize the equations about the uniform distribution and show that one can obtain a dispersion relation that predicts the wavelengths of the maximally unstable modes. We then confirm the linear analysis with numerical simulations of the fully nonlinear system. We note that the dispersion relation that we obtain depends only on the magnitude of the perturbation modes. Therefore, the linear analysis cannot differentiate between parameters that yield stripes or cells. To break the symmetry in the simulations, we also show that if the domain is longer in one direction, it is possible to observe stripes as well as cells.

4. Linear stability

In this section, we consider the linear stability of the two-dimensional veil immersed in a three-dimensional fluid. For our computations, the domain is a square $([0, .5] \times [0, .5])$. To analyze the stability of the homogeneous distribution of bacteria, we expand the free and bound bacterial concentrations as

$$n_b = n_b^0 + \sum_{q_x, q_y} A_{q_x q_y} e^{\gamma t} \cos(q_x x_0 + q_y y_0), \quad (14)$$

where n_b^0 is a constant and $A_{q_x q_y}$ is the amplitude of the different modes.

Expanding Eqs. (7), (6), (17), and (18), neglecting to first order in ϵ leads to a linear system of linear equations for the perturbations $n_f^{(1)}$ and $n_b^{(1)}$,

$$(\gamma n_b^1 + k_- n_b^1 - k_+ n_f^1) e^{\gamma t} \cos(q_x x_0 + q_y y_0) = 0, \quad (15)$$

$$((\gamma + q_1^2 + q_2^2 + k_+) n_f^1 - k_- n_b^1) e^{\gamma t} \cos(q_x x_0 + q_y y_0) = P_c n_f^0 \left(\frac{\partial}{\partial x} v_{x,\delta}^{(1)} + \frac{\partial}{\partial y} v_{y,\delta}^{(1)} \right). \quad (16)$$

The terms $v_{x,\delta}^{(1)}$ and $v_{y,\delta}^{(1)}$ denote the order ϵ terms in the x and y components of the velocities. The velocities are zero up to leading order (by symmetry), so the advection term depends on the initial free density and the order ϵ velocities.

To calculate the order ϵ velocities, we need to calculate

$$\mathbf{v}_{x,\delta} = -\frac{\alpha}{8\pi\mu} \int_{-\infty}^{\infty} d\mathbf{x}_0 n_b(\mathbf{x}_0) \mathbf{G}_{x,y}, \quad (17)$$

$$\mathbf{v}_{y,\delta} = -\frac{\alpha}{8\pi\mu} \int_{-\infty}^{\infty} d\mathbf{x}_0 n_b(\mathbf{x}_0) \mathbf{G}_{z,y}, \quad (18)$$

where n_b^0 is a constant.

To calculate the velocity, we will consider one mode, and the total velocity is then given by a sum over all modes. In the nonlinear computations, we truncate this summation. The velocity in the x direction is

$$\begin{aligned} v_{x,\delta} = & \frac{\alpha A_{q_x q_y} \delta}{8\pi\mu} \frac{\partial}{\partial x} \int_{-\infty}^{\infty} \int_{-\infty}^{\infty} \frac{\cos(q_x x_0 + q_y y_0)}{[(x-x_0)^2 + (y-y_0)^2 + (z-z_0)^2]^{1/2}} dx_0 dy_0 \\ & - \left(\delta \frac{\partial}{\partial x} - 2h(h+\delta) \frac{\partial^2}{\partial x \partial z} \right) \frac{\alpha A_{q_x q_y}}{8\pi\mu} \\ & \times \int_{-\infty}^{\infty} \int_{-\infty}^{\infty} \frac{\cos(q_x x_0 + q_y y_0)}{[(x-x_0)^2 + (y-y_0)^2 + (z-z_l)^2]^{1/2}} dx_0 dy_0, \end{aligned}$$

where $A_{q_x q_y}$ represents the amplitude of the different modes. Using the results from Section 4, we can calculate the velocity in the x direction for a single mode. For the fully nonlinear model, we express the velocity as an infinite sum of terms of the form,

$$\begin{aligned} v_{x,\delta} = & -\frac{\alpha q_x A_{q_x q_y}}{8\pi\mu} \sin(q_x x + q_y y) \left(\delta \sqrt{\frac{c_1}{|\mathbf{q}|}} \mathbf{K}_{-\frac{1}{2}}(|\mathbf{q}|c_1) \right. \\ & \left. - \left(\delta - 2h(h+\delta) \frac{\partial}{\partial z} \right) \sqrt{\frac{c_2}{|\mathbf{q}|}} \mathbf{K}_{-\frac{1}{2}}(|\mathbf{q}|c_2) \right), \end{aligned}$$

where $|\mathbf{q}| = q_x^2 + q_y^2$, $c_1 = z - z_0 = \delta$, and $c_2 = z - z_l = 2h + \delta$. \mathbf{K}_α denotes the modified Bessel function. The y component of the velocity is calculated in a similar fashion,

$$\begin{aligned} v_{y,\delta} = & -\frac{\alpha q_y A_{q_x q_y}}{8\pi\mu} \sin(q_x x + q_y y) \left(\delta \sqrt{\frac{c_1}{|\mathbf{q}|}} \mathbf{K}_{-\frac{1}{2}}(|\mathbf{q}|c_1) \right. \\ & \left. - \left(\delta - 2h(h+\delta) \frac{\partial}{\partial z} \right) \sqrt{\frac{c_2}{|\mathbf{q}|}} \mathbf{K}_{-\frac{1}{2}}(|\mathbf{q}|c_2) \right). \end{aligned}$$

Note that $\partial/\partial z = \partial/\partial c_2$. Therefore, the z derivatives of the Bessel function can be calculated using the recurrence relations,

$$\begin{aligned} \frac{\partial}{\partial c_2} (\sqrt{c_2} \mathbf{K}_{-\frac{1}{2}}(|\mathbf{q}|c_2)) &= \frac{1}{2\sqrt{c_2}} \mathbf{K}_{-\frac{1}{2}}(|\mathbf{q}|c_2) + \sqrt{c_2} \frac{\partial}{\partial c_2} \mathbf{K}_{-\frac{1}{2}}(|\mathbf{q}|c_2) \\ &= \frac{1}{2\sqrt{c_2}} \mathbf{K}_{-\frac{1}{2}}(|\mathbf{q}|c_2) - \frac{\sqrt{|\mathbf{q}|c_2}}{2} (\mathbf{K}_{-\frac{3}{2}}(|\mathbf{q}|c_2) \\ &\quad + \mathbf{K}_{\frac{1}{2}}(|\mathbf{q}|c_2)). \end{aligned} \quad (19)$$

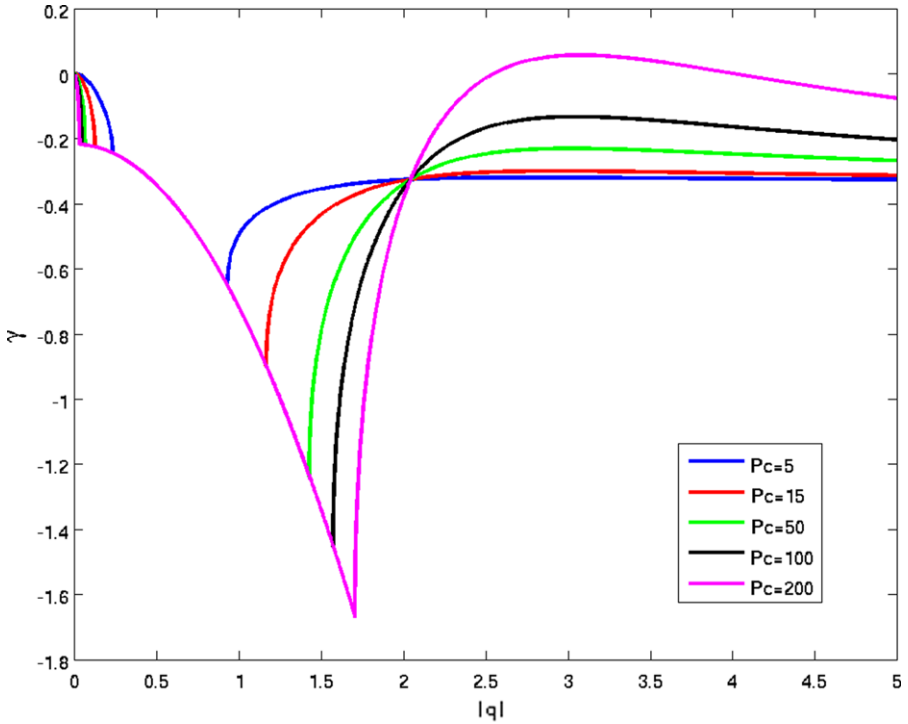


Fig. 2 Example of the dispersion curve for the linearized system. The parameters are $k_+ = 10$, $k_- = 3$ while the Peclet number is varied. We see that as the Peclet number increases from zero the uniform steady-state moves from linearly stable to unstable, with a maximally unstable wave number at approximately 3 for $P_c = 200$.

Using the velocities obtained above in the linearized equations (15) and (16), yields a relationship between γ and the modes of the perturbations. In particular, we use a truncated series approximation for the velocity. This finite series can be used to expand the linearized equations yielding the dispersion curve. Arbitrary perturbations with modes q_x in the x direction and q_y in the y -direction are unstable if the real part of γ is positive. Moreover, the spatial pattern of the unstable mode is determined by q_x and q_y . Rolls occur when only perturbations in one direction lead to positive growth rates while regularly spaced cells occur when neither mode is zero. However, it is clear that the perturbed velocities depend only $|\mathbf{q}|$ which implies that the linear analysis cannot distinguish between rolls and hexagonal patterns. The numerical solution of the fully nonlinear system does capture both regimes.

From the linearized equation, we obtain the dispersion curve, relating the growth rate, given by the real part of γ , to the mode, \mathbf{q} . This relationship is quite complicated, rather than show the exact dispersion relationship, we show a representative plot in Fig. 2.

In the following section, we describe the dynamic behavior of the full system. In particular, we investigate the formation of rolls and cells in various parameter regimes. We note that all the results agree with the linear analysis; namely, regimes where there are

unstable models (Peclet number close to 200), yield nonuniform solutions. We are able to distinguish between rolls and cells in the nonlinear regime.

The magnitude of the force (on the fluid) per unit density of bacteria is equal to the drag coefficient times the swimming speed of a single bacterium, therefore,

$$\alpha \approx 6\pi\mu R V_0,$$

where R is the effective radius of the cell and V_0 is the swimming speed. This implies that $P_c \approx 3h^2 R V_0 n_0 / 4D$, where D is the diffusion coefficient. Since $h \approx 2$ mm, $R \approx 5$ microns, $V_0 \approx 100$ microns/sec, $n_0 \approx 1/400$ (microns)² and a reasonable estimate of D is $D \approx 10^{(-5)}$ (Cogan and Wolgemuth, 2005), we find that

$$\begin{aligned} P_c &\approx 3h^2 R V_0 n_0 / 4D \\ &\approx 10^3. \end{aligned}$$

This estimate helps validate the above analysis, since the experiments imply that the parameters are in the unstable regime (since the uniform veil is only transient).

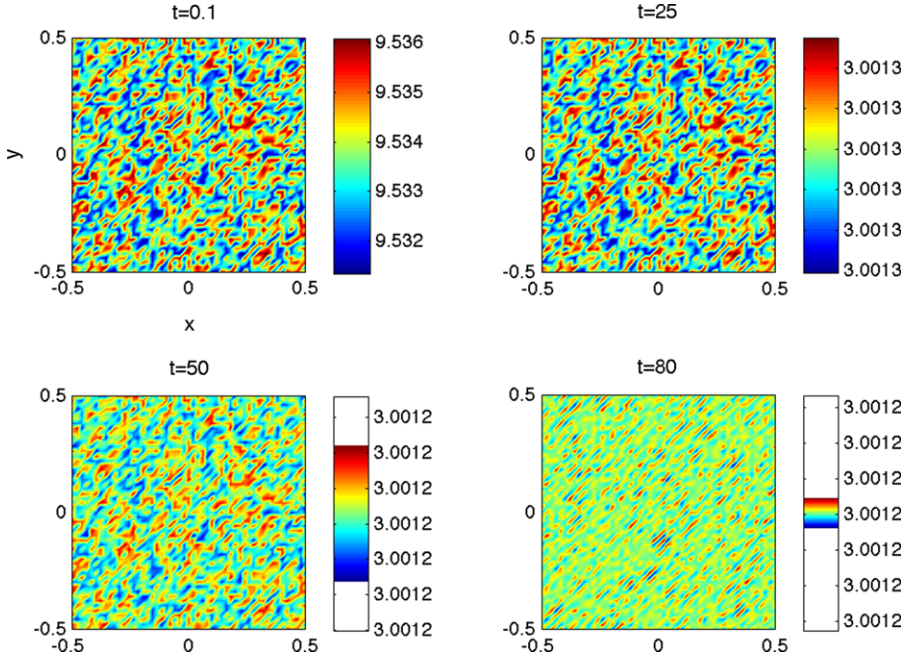


Fig. 3 The dynamics of the system with a square domain, $[-.5, .5] \times [-.5, .5]$ and $P_c = 1$. The uniform steady-state is apparently stable, which agrees with the linear analysis. This can be seen by the color scale, indicating that as time increases, the variation in density decays. Other parameters are $k_+ = 10$, $k_- = 3$.

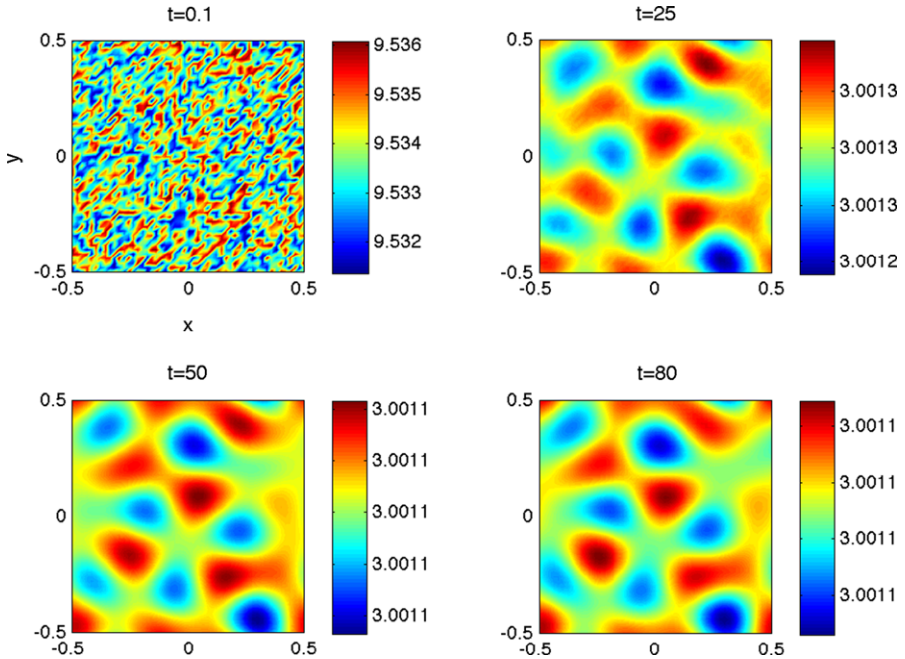


Fig. 4 The dynamics of the system with a square domain, $[-.5, .5] \times [-.5, .5]$ and $P_c = 100$. Considering the color scale, we see that the uniform steady-state is stable. The parameters are $k_+ = 10$, $k_- = 3$.

5. Nonlinear behavior

To investigate the nonlinear behavior, we solve the full equations (7), (6), and (10). We note that there are difficulties in solving these equations on an infinite domain. For practical results, these equations are typically solved on a periodic domain; however to implement this, we need the periodic Green's function. There are several methods available to calculate this in a one-dimensional domain (Pozrikidis, 1992), but the methods do not translate simply into higher dimensions. To avoid this issue, we first embed the domain, $D = (x_1, x_2) \times (y_1, y_2)$ in a periodic collection of N^2 copies of D . We then approximate the behavior on a single domain with periodic boundary conditions to the behavior on the center grid.

On the full grid domain, we use standard methods to solve the equations. The Green's function is well defined and analytic, so that the integrals that yield the velocities can be calculated explicitly on the domain (as in Section A.1). The calculated velocity satisfies Eq. (10), so we are left with solving Eqs. (6), (7), with known velocities. To solve the equations, we use Crank–Nicolson which gives second order accuracy in time and space. In general, we use a 70×70 grid for the square sub-domain $(-.5, .5) \times (-.5, .5)$ and 70×210 grid for the rectangular subdomain $(-.5, .5) \times (-1, 1)$. By computing both a full and half time-step of Crank–Nicolson, provides an error estimate. In general, we use a time step of $dt = 0.01$. We set the tolerance of the error to 10^{-4} and reduce the time step by half if this tolerance is not met.

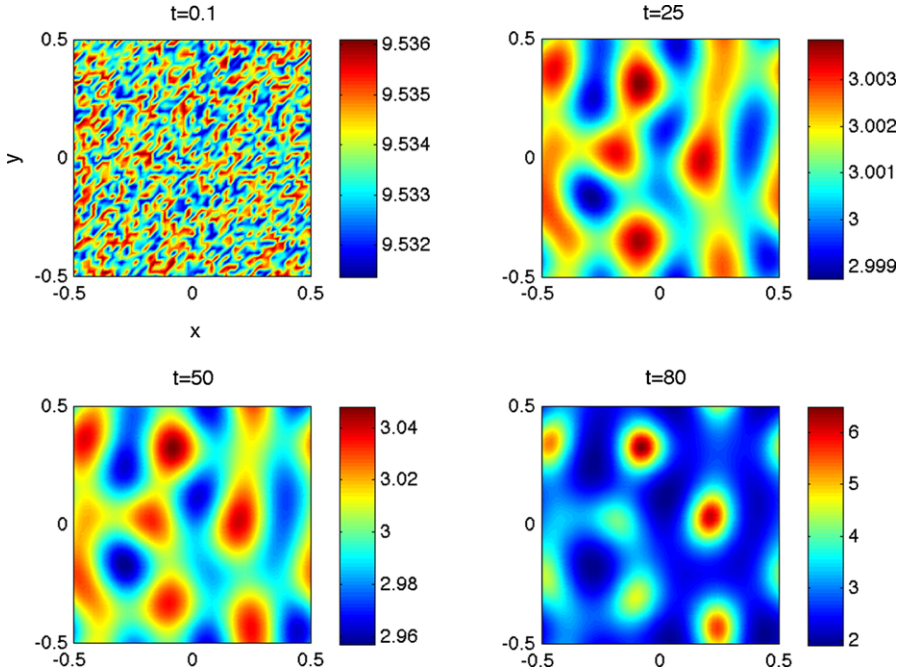


Fig. 5 The dynamics of the system with a square domain, $[-.5, .5] \times [-.5, .5]$ and $P_c = 200$. Here, the uniform state is unstable (as seen by an increase in the variation of the density) and the maximally unstable modes yields the development of spatial patterns. Other parameters are $k_+ = 10$, $k_- = 3$. The Peclet number large enough that the linearized system is unstable, agreeing with the nonlinear computations.

5.1. Spots

We first study the development of spatial patterns on a square domain ($x_1 = -.5$, $x_2 = .5$, $y_1 = -.5$, $y_2 = .5$) using the Peclet number as the control parameter. Recalling that the dispersion curve (see Fig. 2) indicates that for small Peclet numbers, the uniform state is stable, while higher values can yield unstable modes. We also comment that increasing Peclet number can be thought of as an increase in the height of the veil above the ocean floor (h) or as an increase in the force each bacteria induces on the fluid (α). This interpretation concurs with experimental observations that veils formed over depressions or formed by stronger swimmers tend to be spatially heterogeneous (Thar and Kühl, 2002, 2003).

We explore the nonlinear dynamics of the system for varying Peclet numbers. In Figs. 3, 4, and 5, we show snapshots of the system at various times. We clearly see how quickly the system moves from the uniform state when it is perturbed by a small random amount.

We can also visualize the flow associated with the patterns. In Fig. 6, we show cross-sections of the flow in three dimensions. The stream lines are indicated, with the color indicating the velocity. We see representative flows that are essentially radially symmetric near the aggregated attached bacteria agreeing with the imposed flow in Thar and Kühl

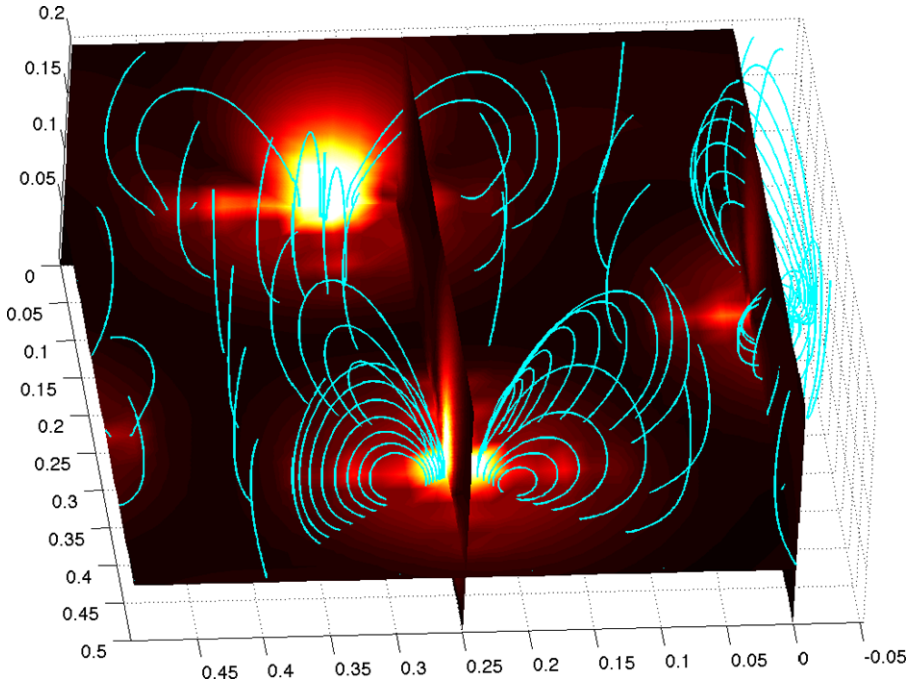


Fig. 6 A snapshot of the three-dimensional flow patterns. The lines show the streamlines of the flow and the magnitude is shown by the color map, with white being fastest flow. The flow field matches the schematic shown in Fig. 1. This figure shows 1/4 of the full domain.

(2006). Near the veil, the flow is transverse and above the veil we see the characteristic reversal in the streamlines bringing the free bacteria back to the veil.

5.2. Stripes

We now investigate the development of stripes. Because of the similarity of the system and analysis to that of the well-known convection instability, it seems clear that there are parameter regimes which tend toward a stable striped configuration. However, the linear theory cannot address this since the dispersion relation depends only on $|\mathbf{q}|$. One way to force the development of stripes is to break the symmetry of the domain. By elongating the y -direction and adjusting the Peclet number, we can find parameter regimes for which the x -direction is too small to allow an instability in that direction while the y component of the domain is large enough to allow for an instability. Specifically, we set $x_1 = 0$, $x_2 = .5$, $y_1 = 0$, $y_2 = 1$. In this domain and for the appropriate Peclet numbers, the stripe steady-state is found.

As before, the uniform state is apparently stable for low Peclet numbers (Figs. 7, 8). As the Peclet number increases, some modes become unstable. Figure 9 show snapshots of the attached bacteria for larger Peclet number ($P_c = 200$). Here, the system is clearly not moving toward the uniform state, but to a striped pattern.

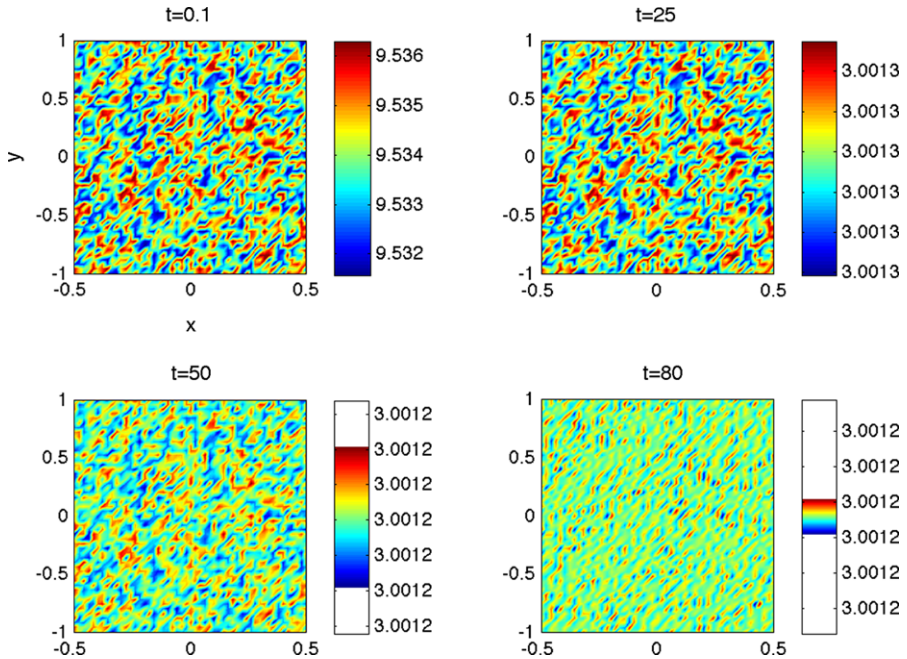


Fig. 7 The dynamics of the solution of the fully nonlinear system with a rectangular domain, $[-.5, .5] \times [-1, 1]$ and $P_c = 1$. The uniform state is stable and the initial perturbation decays. All parameters are the same as the symmetric case.

6. Discussion

We have derived the equations that describe the dynamics and pattern formation of a two-dimensional bacterial veil immersed in a three-dimensional fluid. Linear stability analysis of this system shows that a uniformly dense colony of bacteria will go unstable when the Peclet number for the system exceeds a certain value. This Peclet number is primarily dependent on the height of the veil off the ocean floor and the thrust force that is generated by an individual swimming bacteria. The height of the veil also strongly determines the maximally-unstable mode of the system, and therefore patterns have a characteristic lengthscale that is correlated with the height of the veil. Simulations show that rolls and hexagonal patterns are possible.

As mentioned before, the sulfur-oxidizing bacteria are fairly fast swimmers, with velocities of at least $50 \mu\text{m/s}$ and as high as $600 \mu\text{m/s}$ (Thar and Khl, 2002; Muyzer et al., 2005), whereas *E. coli* has a maximum velocity of only $30 \mu\text{m/s}$. We speculate that one benefit of such high swimming speeds is the generation of the instability that leads to the convective patterns described here. As we noted, a uniform layer of bacteria will not produce any flow. Therefore, to achieve the downward flows through the bacterial colony that bring in oxygen-rich fluid, the bacterial system must have a Peclet number large enough to produce the instability. One way to achieve this large Peclet number is to increase the swimming speed, as fast swimming translates to a larger force exerted on the fluid by the attached bacteria.

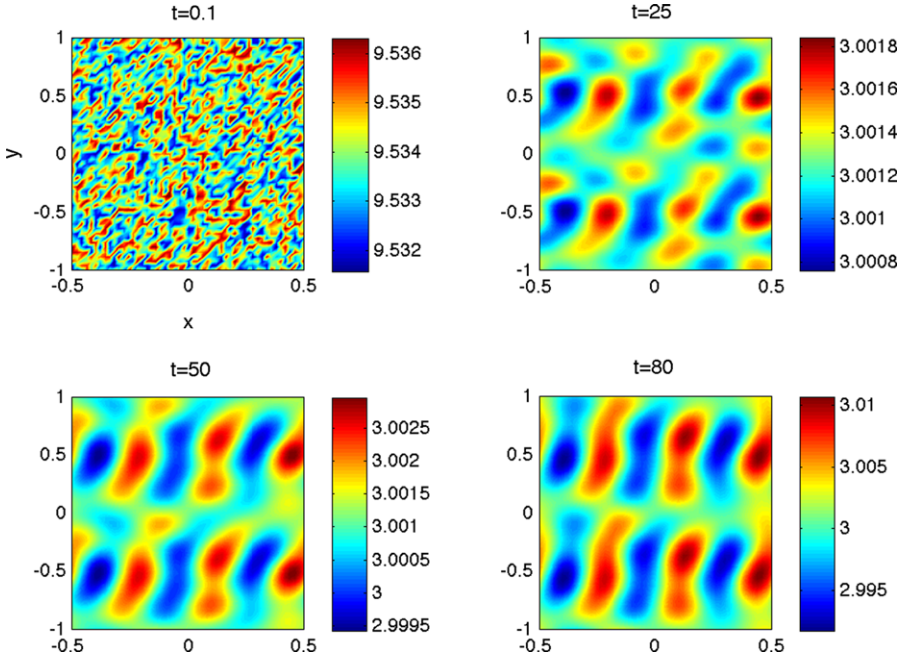


Fig. 8 The dynamics of the solution the fully nonlinear system with a rectangular domain, $[-.5, .5] \times [-1, 1]$ and $P_c = 100$. The uniform state is stable, although there is a weak striped pattern that is transient apparent in the lower right.

We have made several simplifying assumptions in the course of the analysis. One of the most obvious is the absence of any chemotaxis module. In fact, the free bacteria move only in a two-dimensional manner in the current model. A model that accounts for the full, three-dimensional swimming trajectories of the bacteria would be quite complicated and would not be expected to affect the qualitative behavior of the model. Therefore, we have neglected this aspect in the current model. Pattern formation due to local oxygen depletion by the bound bacteria and the consequent aerotaxis may also affect the patterns in this model. Our model, however, shows that these effects are not required to produce the observed patterns. We, therefore, expect that effects from these processes are small. A second simplification concerns the interaction between the veil and the fluid. Instead of a passive veil, it would be more realistic to include a semipermeable interaction. This would alter the local height of the veil making the fluid velocity field more complicated. We have focused our attention on the dominant processes and the analysis of current model reflects the experimental observations.

Appendix

A.1 Calculating the integrals

For the 3D veil linear stability analysis, we need to calculate the velocity field that is generated by a doubly-periodic perturbation in the bound bacterial density, $n_b =$

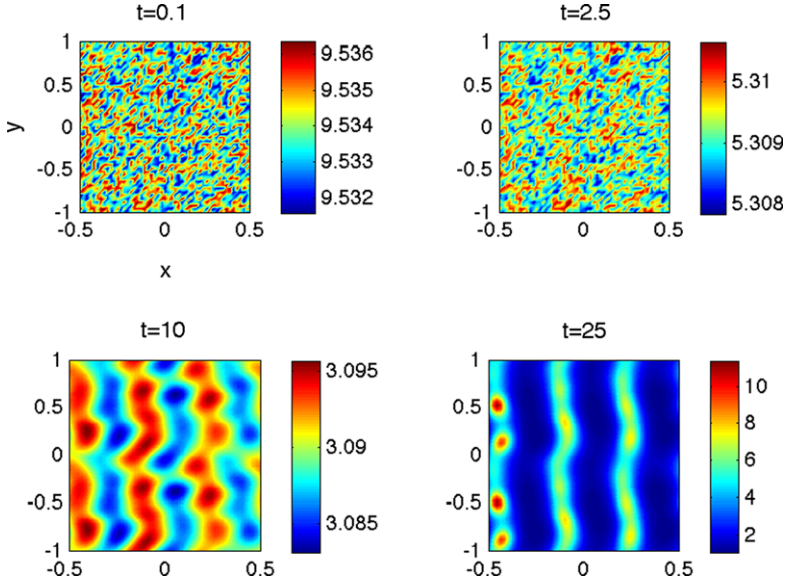


Fig. 9 The dynamics of the solution the fully nonlinear system with a rectangular domain, $[-.5, .5] \times [-1, 1]$ and $P_c = 200$. The Peclet number is sufficiently high so that there is an unstable mode, that is dominated by differentiation in the x -direction.

$n_b^0 \cos(q_x x_0 + q_y y_0)$, where q_x and q_y are the wave numbers for the perturbation in the x and y -directions, respectively. Since the Greens function for bounded fluid motion can be defined using a generating function, it is possible to calculate the double integrals of the generating function and then take derivatives with respect to x , y , and z to get the velocity that is created by the infinite distribution of bound bacteria. Therefore, we need to calculate the integral,

$$\int_{-\infty}^{\infty} dy_0 \int_{-\infty}^{\infty} dx_0 \frac{n_b^0 \cos(q_x x_0 + q_y y_0)}{((x - x_0)^2 + (y - y_0)^2 + (z - z_0)^2)^{1/2}}. \quad (\text{A.1})$$

Making the substitutions $u = (x_0 - x)$ and $c^2 = (y - y_0)^2 + (z - z_0)^2$ and using trig identities, we rewrite this integral as

$$n_b^0 \int_{-\infty}^{\infty} dy_0 \int_{-\infty}^{\infty} du \frac{\cos(q_x u) \cos(q_x x + q_y y_0) - \sin(q_x u) \sin(q_x x + q_y y_0)}{(u^2 + c^2)^{1/2}}. \quad (\text{A.2})$$

The integral containing $\cos(q_x u)$ is a Bessel function, and the term containing $\sin(q_x u)$ integrates to zero:

$$2n_b^0 \int_{-\infty}^{\infty} dy_0 \cos(q_x x + q_y y_0) \mathbf{K}_0[q_x ((y - y_0)^2 + (z - z_0)^2)^{1/2}]. \quad (\text{A.3})$$

To solve this integral, we make the substitutions $v = (y_0 - y)$ and $c = z - z_0$. Using simple trigonometric identities, we get the integral into the form

$$2n_b^0 \int_{-\infty}^{\infty} dv (\cos(q_y v) \cos(q_x x + q_y y) - \sin(q_y v) \sin(q_x x + q_y y)) \mathbf{K}_0[q_x (v^2 + c^2)^{1/2}]. \quad (\text{A.4})$$

As in the previous case, the term containing $\sin(q_y v)$ integrates to zero. The other term can be integrated using 6.726 from Gradshteyn and Ryzhik (1980). We find that Eq. (A.1) becomes

$$n_b^0 \sqrt{\frac{8\pi c}{|\mathbf{q}|}} \mathbf{K}_{-\frac{1}{2}}(|\mathbf{q}|c) \cos(q_x x + q_y y), \quad (\text{A.5})$$

where $|\mathbf{q}|^2 = q_x^2 + q_y^2$.

References

- Batchelor, G., 1967. *An Introduction to Fluid Dynamics*. Cambridge University Press, Cambridge.
- Berglen, T.F., Berntsen, T.K., Isaksen, I.S.A., Sundet, J.K., 2004. A global model of the coupled sulfur/oxidant chemistry in the troposphere: The sulfur cycle. *J. Geophys. Res.* 109, 1–27.
- Blake, J.R., 1971. A note on the image system for a stokeslet in a no-slip boundary. *Proc. Camb. Philos. Soc.* 70, 33310.
- Cogan, N.G., Wolgemuth, C.W., 2005. Pattern formation by bacteria-driven flow. *Biophys. J.* 88, 2525–2529.
- Cortez, R., 2001. The method of regularized stokeslets. *SIAM J. Sci. Comput.* 23, 1204–1225.
- Fenchel, T., Glud, R.N., 1998. Veil architecture in a sulphide-oxidizing bacterium enhances countercurrent flux. *Nature* 394, 367–369.
- Gradshteyn, L.S., Ryzhik, L.M., 1980. *Table of Integrals, Series, and Products*. Academic Press, New York.
- Lorenz, H.A., 1907. Ein allgemeiner satz, die bewegung einer reibenden flussugkeit betreffend, nebst einigen anwendungen desselben, abhand. *Theor. Phys.* 1, 23–42.
- Muyzer, G., Yildirim, E., van Dongen, U., Kühl, M., Thar, R., 2005. Identification of “Candidatus Thio-turbo danicus,” a microaerophilic bacterium that builds conspicuous veils on sulfidic sediments. *Appl. Environ. Microbiol.* 71, 8929–8933.
- Pozrikidis, C., 1992. *Boundary Integral and Singularity Methods for Linearized Viscous Flow*. Cambridge University Press, Cambridge.
- Sass, A., Eschemann, A., Kühl, M., Thar, R., Sass, H., Cypionka, H., 2002. Growth and chemosensory behavior of sulfate-reducing bacteria in oxygen-sulfide gradients. *FEMS Microbiol. Ecol.* 40, 47–54.
- Thar, R., Fenchel, T., 2001. True chemotaxis in oxygen gradients of the sulfur-oxidizing bacterium *Thio-vulum majus*. *Appl. Environ. Microbiol.* 67, 3299–3303.
- Thar, R., Kühl, M., 2002. Conspicuous veils formed by vibrioid bacteria on sulfidic marine sediment. *Appl. Environ. Microbiol.* 68, 6310–6320.
- Thar, R., Kühl, M., 2003. Bacteria are not too small for spatial sensing of chemical gradients: An experimental evidence. *Proc. Natl. Acad. Sci. USA* 100, 5748–5753.
- Thar, R., Kühl, M., 2006. Complex pattern formation of marine gradient bacteria explained by a simple computer model. *FEMS Microbiol. Lett.* 246, 75–79.